Spontaneous Hydrogen Generation from Organic-Capped Al Nanoparticles and Water

Christopher E. Bunker,*,† Marcus J. Smith,‡ K. A. Shiral Fernando,‡ Barbara A. Harruff,‡ William K. Lewis,‡ Joseph R. Gord,† Elena A. Guliants,‡ and Donald K. Phelps†

Air Force Research Laboratory, Propulsion Directorate, Wright−Patterson Air Force Base, Ohio 45433-7103, and Metals and Ceramics Division, University of Dayton Research Institute, Dayton, Ohio 45469

ABSTRACT The development of technologies that would lead toward the adoption of a hydrogen economy requires readily available, safe, and environmentally friendly access to hydrogen. This can be achieved using the aluminum−water reaction; however, the protective nature and stability of aluminum oxide is a clear detriment to its application. Here, we demonstrate the spontaneous generation of hydrogen gas from ordinary room-temperature tap water when combined with aluminum−oleic acid core−shell nanoparticles obtained via sonochemistry. The reaction is found to be near-complete (>95% yield hydrogen) with a tunable rate from 6.4×10^{-4} to 0.01 g of H_2/s/g of Al and to yield an environmentally benign byproduct. The potential of these nanoparticles as a source of hydrogen gas for power generation is demonstrated using a simple fuel cell with an applied load.

KEYWORDS: energy • hydrogen • nanoparticles • aluminum

In obtaining hydrogen from water, it is well-known that aluminum metal will react with water to yield hydrogen gas (1, 2):

$$2Al + 6H_2O \rightarrow 2Al(OH)_3 + 3H_2 \quad (1)$$

$$2Al + 4H_2O \rightarrow 2AlO(OH) + 3H_2 \quad (2)$$

$$2Al + 3H_2O \rightarrow Al_2O_3 + 3H_2 \quad (3)$$

The three reactions represent the products that result from varying water conversion efficiencies (bayerite, boehmite, and aluminum oxide, respectively, with hydrogen). These reactions are limited in their utility because of the natural occurrence of a protective aluminum oxide shell on the surface of the aluminum metal. The stability of the aluminum oxide prevents air and moisture from accessing the underlying metal (3, 4). To circumvent this problem and facilitate the generation of hydrogen, researchers have applied various reaction-promoting schemes. These have included the use of strong bases (5, 6), application of high temperature (7), or activation of the aluminum metal (8−11). Recently, Woodall demonstrated the activation concept and produced large quantities of hydrogen from a gallium−aluminum mixture (8, 9). By dissolving the aluminum in liquid gallium, the researchers prevented the formation of the aluminum oxide shell, thus allowing the aluminum−water reaction to proceed.

* E-mail: christopher.bunker@wpafb.af.mil.

Received for review November 3, 2009 and accepted December 29, 2009

† Wright−Patterson Air Force Base.

‡ University of Dayton Research Institute.

DOI: 10.1021/am900757r

While able to provide hydrogen from the aluminum−water reaction, the above-mentioned approaches are more complex than what eqs 1−3 imply. A simpler solution might be achieved if the nature of the protective aluminum oxide shell could be altered. Recent research on the combustion of aluminum nanoparticles protected by aluminum oxide shells suggests that this may be possible with data demonstrating enhanced reactivity over micrometer- or bulk-scale aluminum (12, 13). These results can be attributed to the role surfaces and interfaces play in nanoparticle chemistry, noting that, as the particle size decreases, the surface and interfacial areas increase and become dominant in determining the physical and chemical properties. Methods for producing aluminum nanoparticles are well-documented (14−24). However, having particles on the nanoscale alone is not sufficient; commercial aluminum nanoparticles possessing an aluminum oxide shell will not readily react in water under ambient conditions. In fact, the mixing of aluminum oxide protected aluminum nanoparticles with water ice has been demonstrated as a stable and viable propellant formulation (25, 26).

To achieve our desired goal, chemical modification of the aluminum oxide shell is also required. Previously, we reported the synthesis of air-stable AlOA core−shell nanoparticles via the sonochemically assisted thermal decomposition of alane in the presence of the catalyst titanium(IV) isopropoxide (18). The physical and thermal analysis of these particles suggested a structure consisting of an inner aluminum core surrounded by an oxide shell, followed by an outer organic shell, each accounting for ~40, 25, and 35% of the total particle mass, respectively. Because the reaction solutions were vigorously deoxygenated prior to the reaction, the oxide shell is believed to have formed from the oxygen atoms brought to the aluminum surface by the capping agent oleic acid. Thermal analysis of the AlOA particles demon-

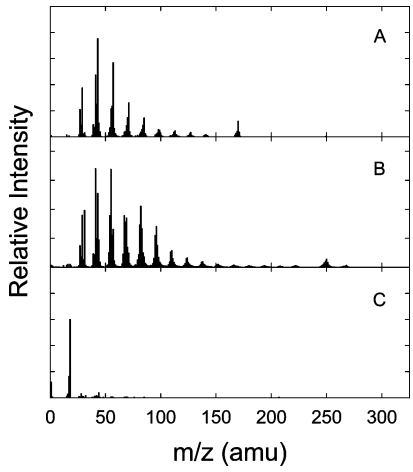

FIGURE 1. TOF mass spectra for the AlOA nanoparticles at (A) 150 °C and (B) 500 °C and for the commercial aluminum nanoparticles with an aluminum oxide coating at (C) 500 °C. The spectra are identified as (A) dodecane, (B) 9-octadecen-1-ol, and (C) water by comparison with the NIST database.

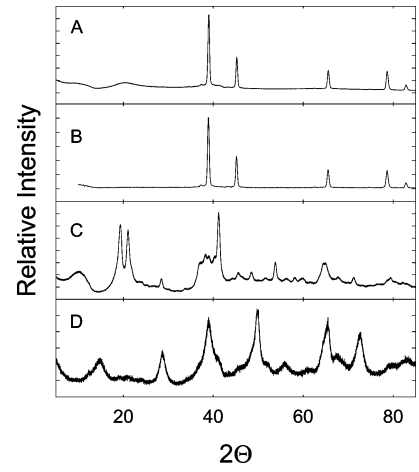

FIGURE 2. Powder X-ray diffraction spectra for (A) the as-synthesized AlOA nanoparticles, (B) the AlOA nanoparticles after exposure to methanol and representative of exposure to hexane, toluene, THF, chloroform, and ethanol, (C) the product of their reaction with water at an AlOA:H_2O ratio of 10^{-3}, and (D) the product of their reaction with water at an AlOA:H_2O ratio of 0.5. The spectra were identified by comparison with the ICPDS database; (A and B) fcc aluminum, (C) a mixture with the main peaks indicating bayerite and boehmite, and (D) boehmite.

strated that this oxide shell does not behave as natural aluminum oxide, instead allowing reaction of the nanoparticles at a much lower temperature (~420 vs 600 °C for commercial aluminum nanoparticles) (18). Using a home-built time-of-flight (TOF) mass spectrometer equipped with a thermal desorption stage, we find that the AlOA nanoparticles release dodecane at temperatures between 100 and 150 °C (Figure 1A) and 9-octadecen-1-ol from ~200 to 500 °C (Figure 1B). The dodecane is a residual solvent entrained in the sample. 9-Octadecen-1-ol is consistent with an oleic acid molecule bound to the aluminum particle through the carbonyl oxygen [RC(OH)OAl] and cleaved between carbon and oxygen. The data correlate well with the observed Fourier transform infrared spectrum, showing a strong O−H stretch and no carbonyl band (18). Commercial aluminum nanoparticles (Alpha Asar) analyzed under the same conditions yield only water vapor (Figure 1C).

The AlOA samples were found to be air-stable; however, to provide a more quantitative measure of the stability, an experimental procedure involving exposure of these samples to air-saturated solvents while agitated in a sonic bath was devised. Specifically, samples (~20 mg) were suspended in a series of solvents (5 mL) and agitated in a sonic bath for 90 min. The solvents included nonpolar hydrocarbons (hexane and toluene), heteroatom and halogenated hydrocarbons [tetrahydrofuran (THF) and chloroform], and polar solvents (ethanol, methanol, and water). In each solvent except one, the particles remained unchanged as measured by powder X-ray diffraction (Figure 2A and 2B). Only water showed a change in the particles with a significantly altered X-ray spectrum (Figure 2C). The spectrum is not identifiable as a single aluminum oxide material, but the main peaks suggest the formation of bayerite and boehmite. To test this reaction, a small quantity of sample was mixed with water and the headspace sampled using the mass spectrometer. After subtraction of a background spectrum, the data showed a strong signal for hydrogen gas (Figure 3). It should be noted that, in the above experiments, the AlOA:H_2O mass ratio is

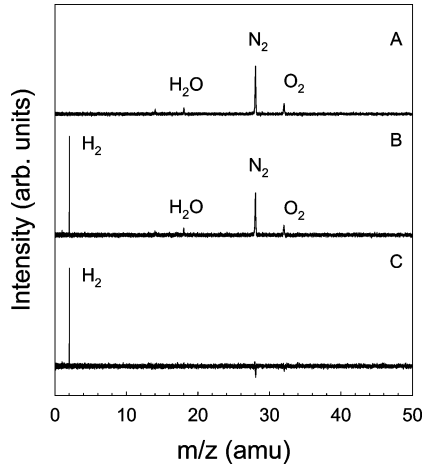

FIGURE 3. Mass spectra demonstrating hydrogen production from reaction of the AlOA nanoparticles and water: (A) background spectrum; (B) reaction spectrum; (C) background-subtracted spectrum.

fairly small (AlOA:$H_2O = 10^{-3}$). When performed at a much larger value (e.g., 0.5), the reaction appeared far more vigorous and generated considerable heat. The X-ray spectrum of the oxide product formed under those conditions is quite different (Figure 2D), demonstrating a clear pattern for boehmite (eq 2).

A second experiment was performed to directly measure hydrogen generation (pressure) versus time. To a 25 mL stainless steel pressure vessel was added 1 g of a AlOA sample and 2 mL of water (AlOA:$H_2O = 0.5$). The pressure is plotted versus time in Figure 4 and shows a rapid rise, which then slows to reach a plateau. The pressure at the plateau is 309 psi, or 21 atm. From the knowledge that our samples are ~40% aluminum metal, using the stochiometery of eq 2 and applying the ideal gas law, we calculate a >95% yield for the formation of hydrogen gas. More importantly, if we examine the rate at which hydrogen gas is generated under continuously reacting conditions (i.e., the

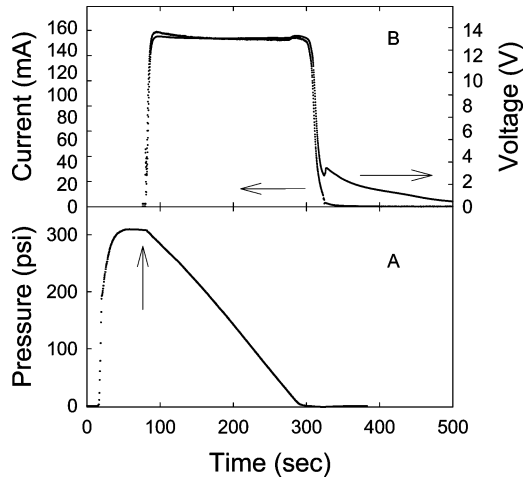

FIGURE 4. Plots of pressure versus time (A) and voltage and current versus time (B) for the reaction of 1.0 g of the AlOA nanoparticles with 2.0 mL of water in a 25 mL stainless steel pressure vessel. The pressure was allowed to stabilize before the fuel cell was brought in line. The operating power was approximately 2 W. In plot A, the arrow indicates the point at which the fuel cell was brought in line. In plot B, arrows indicate the applicable axes.

rapid-rise region), we obtain a rate of ~0.01 g of H_2/s/g of Al. The utility of this hydrogen was also demonstrated in Figure 4, where just after the plateau was reached the pressure vessel was placed in line with a fuel cell (TDM Fuel Cell Technology, 20-stack polymer electrolyte membrane cell) using a pressure regulator set to deliver under 5 psi of hydrogen. Attached to the fuel cell was a simple computer fan to serve as the electrical load, and the voltage and current were recorded as the hydrogen was consumed. As can be seen from the plot, once the hydrogen was delivered to the cell, the voltage and current quickly reached stable working values (~13 V and 0.15 A). The power consumed by this system is ~2 W for a continuous 2.3 min.

Because the reaction appeared to demonstrate a strong dependence on the AlOA:H_2O ratio, a small-scale temperature measurement system was assembled using a thermocouple affixed to an alumina cup to probe this dependence. Water (a constant 60 μL) was added to AlOA samples varying in mass from ~2 to 15 mg (AlOA:H_2O = 0.03−0.25). The temperature was then recorded as a function of time, and the data are plotted in Figure 5. The traces of temperature versus time are all similar in that they exhibit an induction phase, a rapid rise, a maximum, and then a steady decrease, eventually returning to room temperature. The data can be fit using a model that accounts for the heat generated by the reaction q_{rxn}, the heat lost from the system q_{loss}, and the total heat capacity of the system Cp_{total} (a detailed description of the model with definitions for all terms is given in the Supporting Information):

$$T(T) = T(0) + \frac{\int_0^t [q_{rxn}(t) - q_{loss}(t)]\,dt}{Cp_{total}(t)} \qquad (4)$$

The q_{rxn} term is obtained assuming a pseudo-first-order kinetic equation modified to account for the time-dependent surface area (SA) of the reacting nanoparticles:

$$q_{rxn} = \Delta H_{rxn} \int_0^t (1 - e^{-k(t)\,t}) m_{nanoAl}\,dt \qquad (5)$$

where $k(t)$ is

$$k(t) = A\mathrm{SA}(m_{nanoAl})e^{-E_a/RT(t)} \qquad (6)$$

The fits to the data are shown in Figure 5 (fit parameters are also provided in the Supporting Information). From the model, we obtain an average activation barrier of 15 kJ/mol. With this information, we can convert the temperature data in Figure 5 to hydrogen volume versus time and obtain the rate of hydrogen production versus the AlOA:H_2O ratio. The modeled data demonstrate a mass-normalized tunable rate between 6.4×10^{-4} and 5.6×10^{-3} g of H_2/s/g of Al (Figure 5), where the aluminum mass was taken as 40% of the total sample weight. Extending the model to a AlOA:H_2O value of 0.5, we obtain a predicted rate of 0.017 g of H_2/s/g of Al, in very good agreement with the experimentally measured value of ~0.01 g of H_2/s/g of Al (Figure 5).

We have demonstrated that the reaction of aluminum with water to yield hydrogen gas can be performed in a simple fashion, requiring no promoters or initial energy to initiate the reaction. This capability is achieved through the combined effect of using nanoscale aluminum particles coupled with an organic-provided oxide shell, which demonstrates remarkable air and organic solvent stability but allows easy reaction of the aluminum in water. We have shown that the reaction is near-complete, that the rate of hydrogen production can be tuned by controlling the nanoparticle-to-water mass ratio, and that the hydrogen generated by this reaction is sufficient to perform useful work. The simplicity of the reaction, the high energy density of the aluminum−water reaction, and the tremendous stability of these novel aluminum nanoparticles make this system a

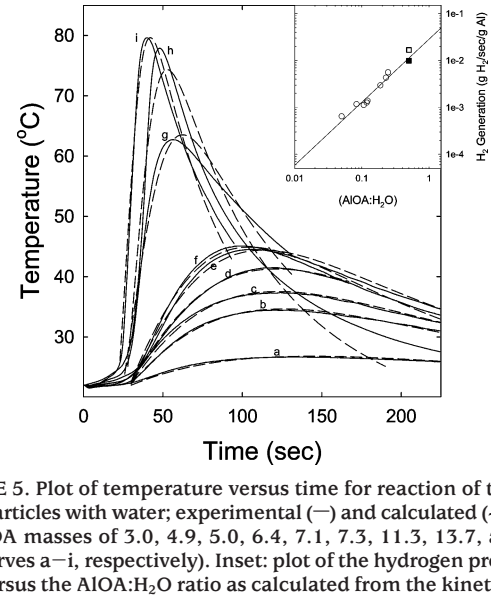

FIGURE 5. Plot of temperature versus time for reaction of the AlOA nanoparticles with water; experimental (—) and calculated (- - -) data for AlOA masses of 3.0, 4.9, 5.0, 6.4, 7.1, 7.3, 11.3, 13.7, and 14.7 mg (curves a−i, respectively). Inset: plot of the hydrogen production rate versus the AlOA:H_2O ratio as calculated from the kinetic model for the data in the main figure (○), calculated for an AlOA:H_2O ratio of 0.5 (□), and measured at a AlOA:H_2O ratio of 0.5 (■).

viable approach for providing power based on hydrogen without requiring the direct storage of large quantities of hydrogen; one need only to add water to produce hydrogen on demand, where and when needed. Future efforts will focus on a better understanding of the nature of the protective shell, the particular role the synthetic method plays in developing these properties, and the effect of the organic capping agent on the reaction parameters.

Acknowledgment. The authors thank Dr. S. Hussain and N. McNamara for helpful discussion and experimental assistance. We acknowledge financial support of the Defense Threat Reduction Agency (Grant HDTRA-07-1-0026), the Air Force Office of Scientific Research through continued support of Dr. Julian Tishkoff, the Air Force Research Laboratory through support of nanoenergetics, and the Dayton Area Graduate Studies Institute for support for M.J.S.

Supporting Information Available: Additional experimental details for the work presented herein, a full description of the kinetic model and definition of all terms, and a table of fit parameters for the data presented in Figure 5. This material is available free of charge via the Internet at http://pubs.acs.org.

REFERENCES AND NOTES

(1) Wang, H. Z.; Leung, D. Y. C.; Leung, M. K. H.; Ni, M. *Renewable Sustainable Energy Rev.* **2009**, *13*, 845–853.
(2) Roach, P. J.; Woodward, W. H.; Castleman, A. W., Jr.; Reber, A. C.; Khanna, S. N. *Science* **2009**, *323*, 492–495.
(3) Vedder, W.; Vermilyea, D. A. *Trans. Faraday Soc.* **1969**, *65*, 561–584.
(4) Digne, M.; Sautet, P.; Raybaud, P.; Toulhoat, H.; Artacho, E. *J. Phys. Chem. B* **2002**, *106*, 5155.
(5) Belitskus, D. *J. Electrochem. Soc.* **1970**, *117*, 1097.
(6) Soler, L.; Candela, A. M.; Macanás, J.; Muñoz, M.; Casado, J. *J. Power Sources* **2009**, *192*, 21–26.
(7) Astankova, A. P.; Godymchuk, A. Y.; Gromov, A. A.; Il'in, A. P. *Russ. J. Phys. Chem. A* **2008**, *82*, 1913–1920.
(8) Cuomo, J. J.; Woodall, J. M. U.S. Patent 4,358,291, Nov 9, 1982.
(9) Cuomo, J. J.; Leary, P. A.; Woodall, J. M. U.S. Patent 4,745,204, May 17, 1988.
(10) Parmuzina, A. V.; Kravchenko, O. V. *Int. J. Hydrogen Energy* **2008**, *33*, 3073–3076.
(11) Deng, Z.-Y.; Liu, Y.-F.; Tanaka, Y.; Ye, J.; Sakka, Y. *J. Am. Ceram. Soc.* **2005**, *88*, 977–979.
(12) Shafirovich, E.; Diakov, V.; Varma, A. *Combust. Flame* **2006**, *144*, 415.
(13) Sun, J.; Pantoya, M. L.; Simon, S. L. *Thermochim. Acta* **2006**, *144*, 117.
(14) Haber, J. A.; Buhro, W. E. *J. Am. Chem. Soc.* **1998**, *120*, 10847–10855.
(15) Jouet, R. J.; Warren, A. D.; Rosenberg, D. M.; Bellitto, V. J.; Park, K.; Zachariah, M. R. *Chem. Mater.* **2005**, *17*, 2987–2996.
(16) Jouet, R. J.; Carney, J. R.; Granholm, R. H.; Sandusky, H. W.; Warren, A. D. *Mater. Sci. Technol.* **2006**, *22*, 422–429.
(17) Foley, T. J.; Johnson, C. E.; Higa, K. T. *Chem. Mater.* **2005**, *17*, 4086–4091.
(18) Fernando, K. A. S.; Smith, M. J.; Harruf, B. A.; Lewis, W. K.; Guliants, E. A.; Bunker, C. E. J. *Phys. Chem. C* **2009**, *113*, 500–503.
(19) Meziani, M. J.; Bunker, C. E.; Lu, F.; Li, H.; Wang, W.; Guliants, E. A.; Quinn, R. A.; Sun, Y.-P. *ACS Appl. Mater. Interfaces* **2009**, *1*, 703–709.
(20) Chung, S. W.; Guliants, E. A.; Bunker, C. E.; Hammerstroem, D. W.; Deng, Y.; Burgers, M. A.; Jelliss, P. A.; Buckner, S. W. *Langmuir* **2009**, *25*, 8883–8887.
(21) Li, H.; Meziani, M. J.; Lu, F.; Bunker, C. E.; Guliants, E. A.; Sun, Y.-P. *J. Phys. Chem. C* **2009**, *113*, 20539–20542.
(22) Weigle, J. C.; Luhrs, C. C.; Chen, C. K.; Perry, W. L.; Mang, J. T.; Nemer, M. B.; Lopez, G. P.; Phillips, J. *J. Phys. Chem. B* **2004**, *108*, 18601–18607.
(23) Kwon, Y.-S.; Gromov, A. A.; Strokova, J. I. *Appl. Surf. Sci.* **2007**, *253*, 5558–5564.
(24) Mahendiran, C.; Ganesan, R.; Gedanken, A. *Eur. J. Inorg. Chem* **2009**, *14*, 2050–2053.
(25) Ingenito, A.; Bruno, C. *J. Propul. Power* **2004**, *20*, 1056.
(26) Risha, G. A.; Son, S. F.; Yetter, R. A.; Yang, V.; Tappan, B. C. *Proc. Combust. Inst.* **2029**, *31*, 2007.

AM900757R